

EmbodiSwap for Zero-Shot Robot Imitation Learning

Eadom Dessalene*, Pavan Mantripragada*, Michael Maynard and Yiannis Aloimonos

Abstract—We introduce EmbodiSwap - a method for producing photorealistic synthetic robot overlays over human video. We employ EmbodiSwap for zero-shot imitation learning, bridging the embodiment gap between in-the-wild ego-centric human video and a target robot embodiment. We train a closed-loop robot manipulation policy over the data produced by EmbodiSwap. We make novel use of V-JEPA as a visual backbone, repurposing V-JEPA from the domain of video understanding to imitation learning over synthetic robot videos. Adoption of V-JEPA outperforms alternative vision backbones more conventionally used within robotics. In real-world tests, our zero-shot trained V-JEPA model achieves an 82% success rate, outperforming a few-shot trained π_0 [1] network as well as π_0 trained over data produced by EmbodiSwap. We release (i) code for generating the synthetic robot overlays which takes as input human videos and an arbitrary robot URDF and generates a robot dataset, (ii) the robot dataset we synthesize over EPIC-Kitchens, HOI4D and Ego4D, and (iii) model checkpoints and inference code, to facilitate reproducible research and broader adoption.

I. INTRODUCTION

Acquiring robot demonstrations for every task, environment, and embodiment is prohibitively expensive, while human video is abundant and easier to gather. Leveraging this, our zero-shot imitation learning approach enables robots to perform new actions without robot demonstrations or goal images, deriving training supervision solely from in-the-wild human video, unlike [2] which depends on curated in-lab demonstrations.

Traditional robot learning generally relies on demonstrations collected via teleoperation, VR [3], or scripted control. Real-world datasets are costly, hardware- and environment-specific, and often severely biased (see Figure 2 in [4]). In contrast, human videos are abundant, diverse, and naturally rich in hand-object interactions. Leveraging large-scale human video not only circumvents the challenges of robot data collection but also broadens the range of actions robots can learn to perform [5].

As robot demonstrations are hard to scale, and large scale human data lacks robot embodiments, we introduce a method - EmbodiSwap - and associated data, which swaps the human embodiment in human video with a robot embodiment. We release a robot manipulation dataset consisting of a large number of robot overlays on egocentric video, here, focusing on its utility for zero-shot imitation learning, though it can support other tasks such as few-shot or inverse RL.

EmbodiSwap transforms human egocentric videos into *robot composited* demonstrations through a multi-step video-

editing process. Hand reconstruction networks recover camera-compensated 3D hand trajectories and produce high-resolution actor masks, which are passed to an inpainting model to remove the human actor and their effects. A photorealistic, pose-aligned robotic hand is composited into the scene using hallucinated depth maps, seamlessly replacing the human actor. Each robot frame is paired with the future end effector pose that drives the action, and these labels are included in the dataset.

We use this data to train closed-loop robot manipulation policies for zero-shot imitation learning. At the core is a video-predictive transformer policy network built on V-JEPA [6], pretrained over 2M human action clips. We freeze V-JEPA’s encoder and fine-tune its predictor and lightweight attention probe. The encoder outputs a representation for each input frame; the predictor combines this with optional proprioception and action tokens, and the probe predicts the robot hand’s future pose, supervised with L1 loss.

During real-world inference we run the policy network in a closed loop: at each step the network outputs an action, the robot executes it, the environment changes, and the new observation is fed back to the network, repeated for a fixed number of steps. Note that during inference our model does not rely on auxiliary goal image conditioning unlike [7].

A considerable body of work has focused on learning robot policies from robot demonstrations [1], [8]. While these methods make good generalist policies capable of following language instructions, they still require in-domain robot data for fine-tuning for new robotic platforms and unseen environments - in contrast our method does not.

We perform an extensive comparison across 13 different pre-trained vision backbones. We observe that V-JEPA pre-trained for video feature-level prediction outperforms all other pre-training methods commonly used within robotics in addition to other non-robotics pre-training methods.

The primary contributions of this work are as follows:

- Novel use of Internet-scale video predictive models towards zero-shot imitation learning. We repurpose V-JEPA, producing a closed-loop manipulation policy, which achieves an 82% real-world success rate over 5 actions. Across all actions we outperform a few-shot trained π_0 model which has access to in-lab robot demonstrations, as well as the zero-shot π_0 model trained over data produced by EmbodiSwap (which outperforms the few-shot trained π_0 model).
- Empirical demonstration of the superiority of using a V-JEPA model pre-trained for feature-level video prediction (a non-standard pre-training method in robot manipulation) over other pre-training methods, for the

* These authors contributed equally to this work.

The authors are with the department of Computer Science, University of Maryland, College Park, MD, 20742

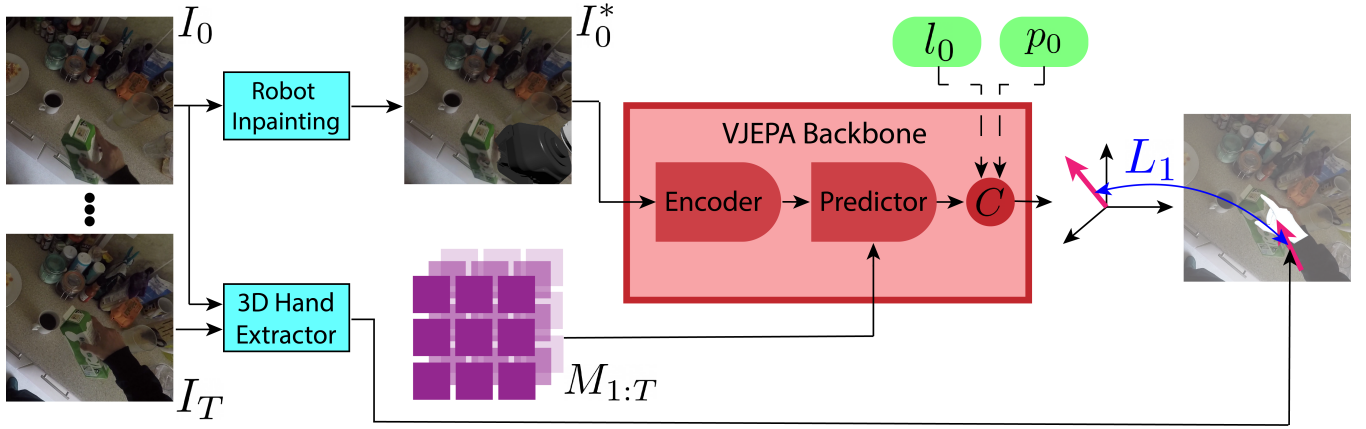


Fig. 1. **Overview of our training setup:** Our system takes a sequence of frames $\{I_0, \dots, I_T\}$ featuring a human actor performing an action as input. The first frame of this sequences is passed to a multi-step **Robot Compositing** process, producing an image I_0^* with the human hand of I_0 substituted with a robot manipulator. The robot image I_0^* is passed into **V-JEPA encoder**. The output of the encoder is passed along with a stack of positional mask tokens $M_{1:T}$ that correspond to frames $I_{1:T}$ to the **V-JEPA predictor**. The output of the predictor is then fed along with optional (represented by dashed lines) encoded representations of proprioception token p_0 and an action location token l_0 (both associated with I_0) into cross-attention layers C . C produces as output a relative hand transform prediction, corresponding to a relative predicted hand transform from I_0 to I_T . Training is supervised using L_1 loss with a training signal of a relative 3D transform of the hand as derived between images I_0 and I_T by the **3D Hand Reconstruction** network. For clarity, model and 3D Hand Reconstruction output are overlayed onto I_T as output in the figure.

purpose of forecasting future end-effector trajectories.

- **EmbodiSwap:** Overlay of robot embodiment over existing egocentric video, as well as temporal boundaries well-suited for robot manipulation tasks, creating a large-scale robot manipulation dataset. We release all training data, checkpoints and inference code here. Given a robot URDF and egocentric videos, we release the code for generating robot-composed videos.

The rest of this paper is structured as follows: In Section II we detail related work, in Section III we detail our method, in Section IV we cover experiments, and in Section V we conclude.

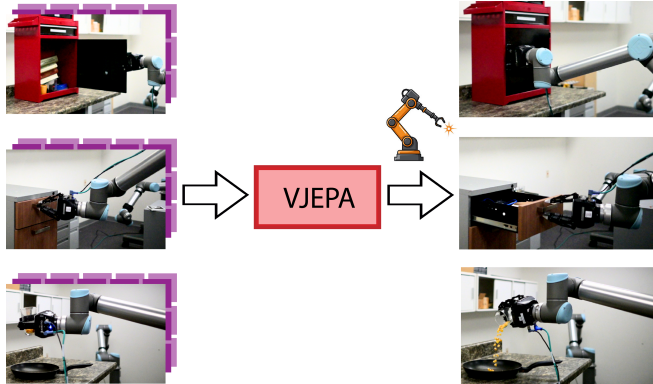


Fig. 2. **Overview of our Zero-Shot test setup:** After training V-JEPA over distributions of scenes, objects, and embodiments, we deploy the network on *out-of-distribution* embodiments, objects and environments. Test sequences — consisting of the first RGB frame plus positional masks for subsequent frames — are provided as input, producing as output a relative transformation predictions. We illustrate three example sequences, one each for: *close*, *open*, and *pour*. Input is shown on the left, and the consequence of action execution is shown on the right.

II. RELATED WORK

A. Forecasting Future Hand Trajectories

Forecasting future hand trajectories is a difficult but essential problem for aligning human and robot actions. Early work by [9] introduced *contact anticipation maps*, per-pixel time-to-contact estimates between hands and objects. [10] predicted 2D hand motion by modeling synergies between hand trajectories and object affordances. More recently, [11] utilizes explicit head motion prediction and additional modalities. However, no prior work has systematically compared state-of-the-art vision backbones for regressing future hand poses. We address this gap by evaluating 13 models, demonstrating the superiority of V-JEPA [6].

B. Learning Robot Policies from Human Videos

The use of large-scale human video datasets for robot policy learning has grown rapidly. Most works [12], [13], [14] leverage such data for visual pre-training, then fine-tune on a smaller (though still large) set of robot demonstrations. More recent approaches [2], [7], [15] explore *zero-shot* learning from human videos without robot demonstrations. Our method differs from [7] by avoiding reliance on a goal image — essentially a partial demonstration — and by addressing the human-to-robot embodiment gap. Unlike [2], [15], we train on *in-the-wild* human data, and through doing so leverage its advantages. [16], while similar in approach, is not zero-shot since it still requires additional robot demonstrations.

III. METHODS

Here we detail our method for zero-shot robot imitation learning from human video. Our model implementation is centered on a fine-tuning of a pre-trained V-JEPA model, the process of which we detail in Section III-A. This is dependent on EmbodiSwap: a multi-step data processing,

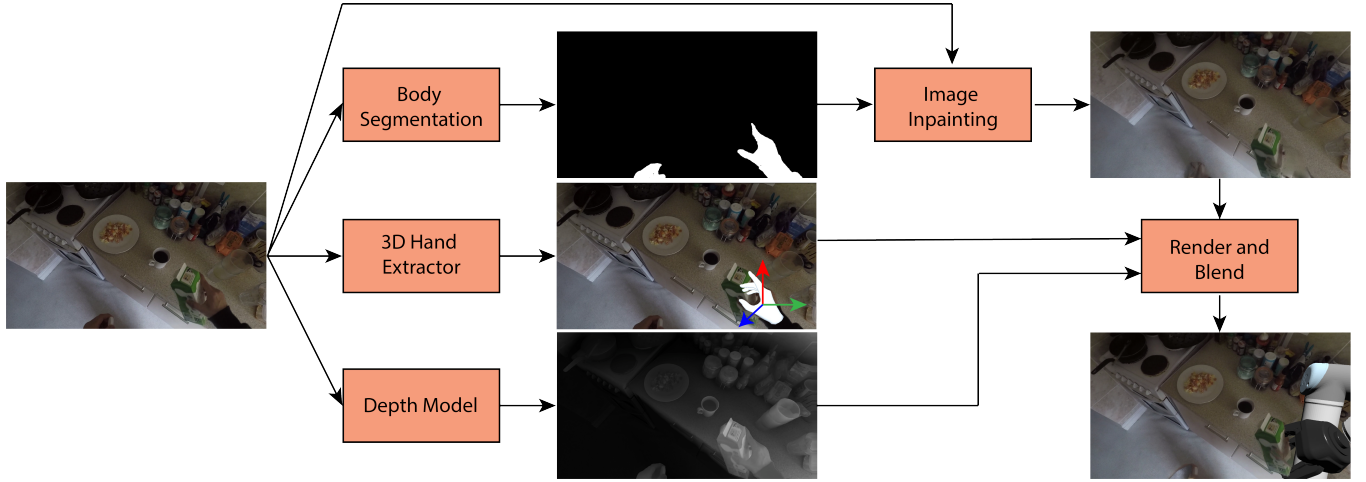


Fig. 3. **Overview of our robot compositing pipeline:** The process begins with a human RGB frame in which a hand is visible. This image is processed first by three components: 1) a **Body Segmentation Network**, which produces a binary segmentation mask of the human actor; 2) a **3D Hand Extractor**, which reconstructs the human hand skeleton in 3D; and 3) a **Depth Network**, which estimates accurate metric depth (composite of grayscaled image and depth image shown for visualization purposes). The output of these components is then further processed by an additional two components: 4) **Image Inpainting**, which takes the original RGB image and the body segmentation and erases the human actor and their effects from the scene. And, finally 5) **Render and Blend**, which takes all of the inpainted image, depth map, and the end-effector pose, and renders a synthetic robot manipulator, composites it into the scene, and adjusts foreground/background contents based on the depth differences between the scene and the robot.

as covered in Section III-B. This involves overlaying robots on human data (III-B.1), which in turn relies on mapping between human and robot effectors (III-B.2), producing targets for training (III-B.3), and re-segmenting human data for robot imitation learning (III-B.4). Finally, the training of this setup over this data is covered in Section III-C.

A. Model Architecture

Here we describe our method’s data and model flow as illustrated in Figure 1.

We primarily leverage 2 components of the V-JEPA backbone architecture from [6]. V-JEPA originally consists of three components: i) an x-encoder (**Encoder** within Figure 1) subnetwork that ingests a masked input video and produces an embedded vector for each non-masked video token, ii) a predictor (**Predictor** within Figure 1) subnetwork that ingests the embedded vectors from the x-encoder along with a set of positional mask tokens each of which corresponds to the masked portion of video, and predicts feature targets for the input video, and iii) a y-encoder subnetwork that takes the entire video and produce deep feature targets. For how V-JEPA is pre-trained, we refer readers to Section 3 of the V-JEPA paper [6].

The input to the V-JEPA policy network consists of a robot composited image I_0^* (whose production is described in Section III-B), $M_{1:T}$ (the positional mask tokens corresponding to frames $I_{1:T}$), and optional proprioception and action location inputs p_0 and l_0 , respectively. Image I_0^* is fed into the V-JEPA encoder, producing an embedding of the image I_0^* . The embedding is fed to the predictor, which uses $M_{1:T}$ to predict an encoded representation of the video $I_{0:T}^*$. Separately, the proprioception input p_0 and action location input l_0 are encoded by fully connected layers. The output of the predictor as well as the encoded representations of p_0

and l_0 are concatenated and then fed into attention probe C consisting of two cross attention layers followed by 2 self attention layers. The final output is fed into a fully connected layer which produces a single relative pose vector, where the training signal is derived as per Section III-B.

B. EmbodiSwap

Human videos are abundant and easy to collect at scale. Furthermore, egocentric video in particular contains a diverse set of cues. The motions of the hands and the objects of interaction are of particular relevance to robotic manipulation. While both are desirable in principle, extracting and modeling the 3D motion of objects poses a number of difficulties and is considerably more error-prone than estimating the 3D motion of hands. Accordingly, we rely primarily on hand motion.

Centering the importance of hands, we substitute human hands with robot manipulators in video clips (Section III-B.1). The resulting data are then used to train the V-JEPA model with a derived training signal (Section III-B.3). Because temporal action boundary annotations in existing action datasets are often ambiguous and inconsistent [17] and ill-suited for robot manipulation learning, we re-annotate these boundaries (Section III-B.4).

1) *Robot Compositing Process:* Given a clip featuring a human actor performing object manipulation, we wish to transform the RGB frames of that clip in such a fashion that they depict a scene featuring a robotic actor mimicking the motions of the human actor. We detail our process - applied framewise - for this substitution in Figure 3. The input RGB frame is fed into: 1) Body Segmentation, 2) 3D hand Extractor, and 3) Depth Model. The human is removed by 4) Image Inpainting, and the robot is overlaid by 5) Render and Blend

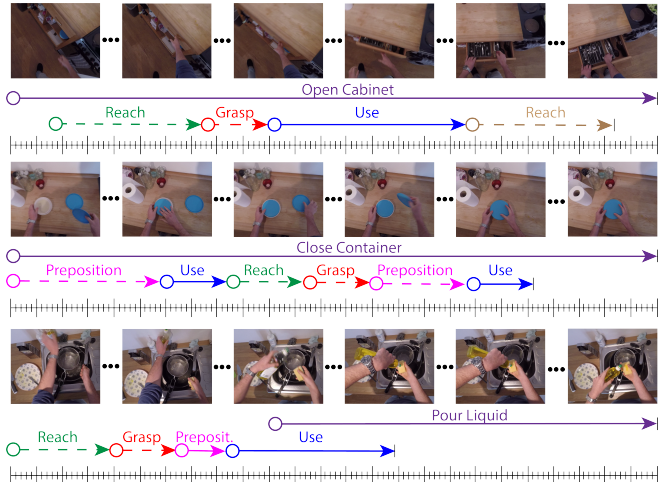


Fig. 4. **Action and sub-action boundaries:** A visualization of 3 example sequences taken from EPIC Kitchens. The top row within each example corresponds to cropped RGB frames. The purple arrow in the middle row corresponds to the ground truth annotated action and its temporal boundaries as provided by EPIC Kitchens. The (red, green, blue, pink, and tan) arrows in the third row correspond to the sequences of Therblig sub-actions, and their temporal boundaries. Both solid and dashed arrows indicate the temporal extend of Therblig sub-actions. A dashed arrow indicates that the Therblig sub-action is extraneous, and a solid arrow indicates that the associated sub-action clip is used in training our system. We release our annotations publicly here.

We extract the 3D hand trajectory of the hand of interaction, using HaWoR [18], a 3D reconstruction method that jointly reconstructs the 3D hands and camera pose for each frame. We also feed the entirety of the clip to the frame-wise depth model UniDepthV2 [19], a network that takes frames along with intrinsics and produces metric valued depth estimates.

Additionally, each frame is fed to a Body Segmentation network that produces a binary mask capturing all pixels that belong to the body of the actor. To generate a high resolution body segmentation mask, we utilize SAM2 [20], prompted with points belonging to the body from a coarse segmentation of the original image in low-resolution (provided by a network trained over VISOR [21]). The binary segmentation output in addition to the original frame are then passed into OmniEraser [22], a high-resolution Image Inpainting network that produces an image of the scene absent of the actor and their effects.

The output of these components are then blended, and a final image render in Render and Blend: We re-target the 3D hand extracted from each frame into a gripper pose vector (detailed in Section III-B.2). We then render an RGB-D synthetic robot at the derived gripper pose using Pybullet’s IK. The depth maps belonging to the scene are pixel-wise compared to the rendered depth map belonging to the synthetic robot, where we blend the corresponding inpainted image and the synthetic robot image by selecting for pixels with the smaller depth values between the two maps, yielding an image of a robot manipulator in place of the original human actor.

We compare the scene’s depth map to the robot’s rendered

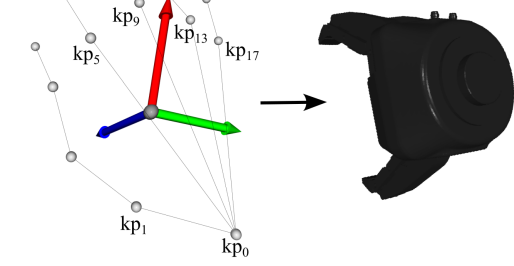


Fig. 5. **Human Hand Pose to Gripper Pose Re-targeting:** On the left we extract the MANO joint positions of the human hand. From this we extract a 6-DOF hand pose. We then align the robot gripper - on the right - to conform to this derived 6-DOF hand pose.

depth map, pixel by pixel. At each pixel, we choose the source with the smaller (nearer) depth to blend the inpainted scene and the robot render. The final result is an image where the robot manipulator replaces the original human actor, while allowing for occlusions on top of the robot manipulator (e.g., by the object).

2) *Gripper Pose Re-Targetting:* 3D human hand skeletons, as shown in Figure 5, extracted from video frames cannot be directly applied to a robot due to the embodiment gap. To ensure that the robot videos generated from human demonstrations exhibit physically plausible gripper poses, we use MANO [23] parameters predicted by the HaWoR model in modeling the human hand and subsequently re-target the gripper pose.

Our re-targeting scheme supports both two and three-finger grippers. Given the MANO parameters, we compute the 21 joint points kp_i , $i \in [0, 20]$. The gripper center is defined as the human palm center, $\mathbf{G}_c = \frac{1}{5}(kp_1 + kp_5 + kp_9 + kp_{13} + kp_{17})$. The gripper orientation is set as follows: The gripper Z -axis is aligned with the normal to the human palm, $\mathbf{G}_z = (kp_5 - kp_0) \times (kp_{17} - kp_0)$. The gripper X -axis is aligned with the vector from the first thumb joint of the human to the centroid of the first joints of the remaining fingers, $\mathbf{G}_x = \frac{1}{4}(kp_5 + kp_9 + kp_{13} + kp_{17}) - kp_1$. For the Y -axis, we set $\mathbf{G}_y = \mathbf{G}_z \times \mathbf{G}_x$ when mapping to the right hand and $\mathbf{G}_y = -\mathbf{G}_z \times \mathbf{G}_x$ for when mapping to the left hand. The resulting gripper pose $\mathbf{T}_g = [\hat{\mathbf{G}}_x \hat{\mathbf{G}}_y \hat{\mathbf{G}}_z \mathbf{G}_c]$ is used both for in-painting the robot and as the regression target for our model.

3) *Ground Truth:* When building the end-effector targets we train our policy network over, we take each video frame and pair it with the hand pose from a future frame. The look-ahead (in frames) varies by action: we use a shorter offset for rapid hand motions (e.g. *open*, *close*) and a longer one for slower movements, such as *pouring*. We compute the relative translation and rotation between the hand pose for the current frame and the hand pose from the future frame as a 6D pose.

4) *Robot Manipulation Action Boundaries:* Different temporal segmentations give different motions. Because we’re

learning motion, it's important to have precise and consistent temporal segmentation. Existing temporal action boundaries for our data are annotated for action classification which is temporally ill-defined [17]. To address this, we provide re-annotated temporal boundaries that segment actions based exclusively on hand motion, as shown in Figure 4. To this end we annotate according to the Therblig sub-action ontology. Therbligs are a low-level mutually exclusive contact demarcated set of sub-actions. For a depiction of Therbligs and their usage, see Figure 1 within [24]. In addition to the revised action boundaries, annotators are to indicate the dominant hand of interaction which is missing from existing egocentric datasets.

C. Training and Deployment

After running the robot compositing process over the human images, we arrive at the robot images to be fed into the V-JEPA network. These are paired with the corresponding future hand poses derived in Section III-B.3. The V-JEPA network when fine-tuned over action classification tasks typically ingests video input [6] - we observe that the training of V-JEPA over video input marginally hurts performance as compared to a single frame input, as shown in the comparisons within Table I. For more training details, see Section IV-B.

We deploy our trained policy network in the real-world as shown in Figure 2. There is a difference in appearance between the robot embodiment as rendered in our simulated training data, and the physical robot platform we evaluate over during deployment in the real world. To circumvent this we use the joint angles of the physical robot and render a synthetic RGB image of the physical robot. We overlay this synthetic image over the input image, in a process analogous to that shown in Figure 3. However, we observe that empirically this substitution is largely unnecessary - the model predictions change only marginally due to this substitution. A square crop from the synthesized image is fed to V-JEPA. The policy network then produces as output a relative transform for the robot's end effector to follow.

IV. EXPERIMENTS

Here we detail our experimental evaluation. Data is characterized in Section IV-A, and training details are provided in Section IV-B. We provide an assessment over pre-training methods in Section IV-C, demonstrating the superiority of feature-level video prediction pretraining over other pre-training methods. In Section IV-D we present evaluations performed using a physical platform in our lab.

A. Data

We model actions most frequently labeled within the action datasets - in this case, *placing*, *opening*, *closing*, *pouring* and *cutting*. We source videos from 3 popular egocentric datasets - EPIC Kitchens [32], HOI4D [33] and Ego4D [34]. We source all five actions from EPIC Kitchens 2020, *placing*, *opening* and *closing* actions from HOI4D and *pouring* and *cutting* videos from Ego4D.

When prompting annotators to re-annotate boundaries of action clips as in Section III-B.4, we define actions to begin when the tool object is *grasped*, and terminate before the end of the *use* operation, which corresponds to the post-condition of the action being satisfied (e.g. door finishes *opening/closing*, cuttable object is sliced, etc).

We do training and evaluation over the different actions independently, as opposed to pooling the different actions into a single dataset. For the *open*, *close*, and *cut* action, we make no use of the action location as input to the network, feeding a placeholder instead. For the *pour* action, we feed a noisy estimate of the action location as input so as to encourage the network to be rely on visual cues for the *pouring* action. For all actions, except the *place* action, we include proprioception to the network - for the *place* action, we observe that the network performs better when denied access to proprioception information.

B. Training Details

We resize images from the original resolutions to a fixed resolution of 1080×1920 . During training we apply random crops (scales range from 0.4 to 0.99) and random horizontal flips, which we find helps generalization for all actions (non-spatial augmentations such as color augmentations tend to hurt generalization). Cropped images are then resized to resolution 224×224 and fed into the policy network.

For the results reported in Section IV-C, we freeze all layers except the attention probe. For the results reported in Section IV-D (and in accordance with Figure 1, we only freeze the encoder, training the predictor as well as the attention probe.

We train our policy network for 40 epochs with a batch size of 32, an initial learning rate of $1e-3$, and a cosine scheduler that ends the learning rate at $1e-7$. We also adopt a weight decay of 0.01. Because we keep the V-JEPA encoder backbone frozen, we are able to achieve the memory requirements of the single RTXA5000 GPU we use for training.

C. Pre-training Method Comparisons

Here we wish to evaluate the impact of the selection of different pre-training methods for the final task of end-effector pose prediction. A pre-training method is categorized based on which supervision category, modality type, and data type it employs, as specified in Table I. This is important to explore as it determines the extent to which advancements in vision can be transferred directly into robot learning. The data input are the robot images produced by EmbodiSwap, and the ground truth are their paired future poses.

We choose a suite of pre-trained vision backbones for comparison associated with state-of-the-art vision models. In these experiments we follow the convention of [6] in swapping out the encoder-predictor subnetworks for the vision backbone of the evaluated model. The attention probe operates over the frozen features produced by the evaluated model, identically as in Section III-A. For simplicity, we keep the vision backbones frozen to allow for identical learning

Model	Supervision	Pretrained Modality	Data type	Open		Close		Pour		Cut		Place	Composite Trans	Composite Rot
				Trans	Rot	Trans	Rot	Trans	Rot	Trans	Rot			
ResNet-50	supervised	image	non-robot	0.119	0.394	0.115	0.412	0.083	0.358	0.061	0.250	0.167	0.109	0.354
MAE ViT-B/16 [25]	self-supervised	image	non-robot	0.089	0.342	0.095	0.342	0.071	0.312	0.057	0.247	0.147	0.092	0.311
DINOv2 [26]	self-supervised	image	non-robot	0.084	0.359	0.094	0.369	0.071	0.301	0.051	0.251	0.119	0.084	0.320
R3M [27]	supervised	image	non-robot	0.109	0.401	0.116	0.37	0.099	0.415	0.061	0.262	0.178	0.113	0.362
ViP [28]	self-supervised	image	non-robot	0.110	0.376	0.119	0.444	0.106	0.399	0.065	0.345	0.192	0.118	0.391
VC-1 [29]	self-supervised	image	non-robot	0.101	0.372	0.104	0.385	0.080	0.326	0.0584	0.249	0.139	0.096	0.333
Octo [8]	supervised	image	robot	0.147	0.415	0.138	0.392	0.085	0.363	0.062	0.273	0.220	0.130	0.361
RoboFlamingo [30]	supervised	image	robot	0.139	0.430	0.140	0.391	0.083	0.371	0.0599	0.340	0.169	0.226	0.383
π_0 [1]	self-supervised	image	robot	0.102	0.361	0.104	0.36	0.089	0.336	0.054	0.235	0.160	0.102	0.323
ResNet-3D	supervised	video	non-robot	0.110	0.416	0.109	0.373	0.095	0.315	0.048	0.331	0.195	0.111	0.359
Hiera-L [31]	self-supervised	video	non-robot	0.092	0.363	0.104	0.399	0.071	0.296	0.050	0.290	0.155	0.094	0.337
V-JEPA + T (ViT-L)	self-supervised	video	non-robot	0.085	0.338	0.081	0.280	0.065	0.239	0.049	0.239	0.101	0.076	0.274
V-JEPA (ViT-H)	self-supervised	video	non-robot	0.086	0.319	0.080	0.334	0.061	0.256	0.042	0.236	0.094	0.073	0.286
V-JEPA (ViT-L)	self-supervised	video	non-robot	0.082	0.335	0.082	0.269	0.069	0.260	0.045	0.236	0.099	0.076	0.275

TABLE I. Pre-training Method Comparison: Here we evaluate the utility of different pre-training methods trained over EmbodiSwap data for the task of forecasting end-effector pose, over the following actions: *Open*, *Close*, *Pour*, *Cut* and *Place*. We define pre-training method according to Supervision, Modality, and Data Type categories. Supervision is broken into classification (whether it be object or action classification), self-supervision (where the training signal is derived from input), and action prediction (regression of end-effector pose). Modality can be either image or video. Data type is either robotic data, non-robotic data, or a mix of both. We present the final model performance across 5 actions independently, as well as in aggregate. For each, performance is divided into translation prediction error (in meters), and rotation prediction error (unitless). For models pretrained over images, we use images alone. For models pretrained over videos (except VJEPAs), we use images cloned across the temporal dimension. For V-JEPA + T we use video sequences. For V-JEPA (ViT-H and ViT-L) we feed input as per Figure 1.

settings across experiments, only training the attention probe and cross attention layers. We also do not feed in proprioception or action location inputs so as to focus evaluation on the visual backbone.

D. Real-World Experiments

We conduct our experiments on a real-world UR10 robot with a Robotiq gripper controlled using ur_rtde interface [35]. The environment we deploy over is a lab setting with different background and lighting conditions than the kitchen environments the policy network is trained over (illustration

TABLE II
REAL WORLD ROBOT EVALUATION: COMPARISON OF 3 DIFFERENT MODELS (SECTION IV-D FOR DETAILS). 30 REFERS TO TRAINING OVER 30 IN-LAB DEMONSTRATIONS. ES REFERS TO EMBODISWAP. OUR METHOD IS V-JEPA OVER ViT-L WITH EMBODISWAP DATA.

Method	Open	Close	Pour	Place	Cut	All
π_0 (30)	6/20	4/20	2/15	2/15	1/15	15/85
π_0 (ES)	18/20	3/20	1/15	0/15	0/15	24/85
Ours	19/20	17/20	10/15	10/15	14/15	70/85

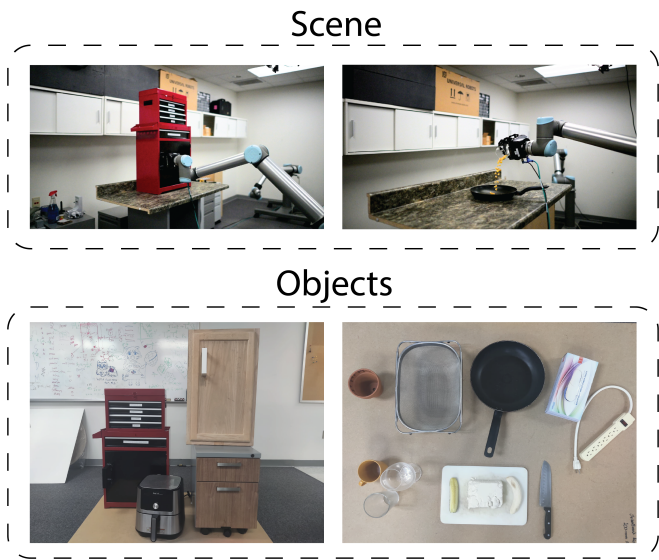


Fig. 6. Real World Experimental Setup: We deploy a UR10 robot in the real world to perform each of the following actions: *open*, *close*, *pour*, *cut* and *place*. The top row depicts *opening* a toolbox on the left side, and *pouring* the contents of a cup into a pan on the right side - the bottom row depicts the objects used for *open* and *close* on the left side, and the objects used for *cut*, *place* and *pour* on the right side.

in Figure 6). Of the 5 actions we demonstrate, 2 of the actions (*open* and *close*) are contact rich in that the robot’s commanded motion is constrained by the articulated joint of the objects of interaction. For these actions, we adopt a force controller that allows compliance in all 6 degrees of freedom, with the tradeoff of precise control. For the remaining three actions (*pour*, *cut* and *place*) we adopt a position controller, which terminates execution upon collision but gives precision in reaching commanded movements.

We evaluate action outcomes using the following criteria: (i) *open* succeeds when a rotational door rotates beyond 65° or if a translational drawer extends more than 80% of its maximum range; (ii) *close* succeeds only when the cover makes contact with the base; (iii) *pour* succeeds when over 80% of the styrofoam pieces (we avoid liquids) fall into the receiving vessel; (iv) *cut* succeeds only when the knife slices through the target object; (v) *place* succeeds when the object makes contact with the point belonging to the designated target location.

To capture the complexity of *place*, we employ large objects (pan, power strip, box, etc.) for manipulation, and initiate the robot grasp of the object on the object periphery,

away from the object centroid. This requires V-JEPA to learn to model spatial relations involving object shape, gripper alignment, and target location. This differs from placing small objects, as small objects can be placed simply by positioning the gripper directly over the target location, requiring neither object nor gripper spatial modeling.

Across trials of *pour* and *cut* tasks, we randomize the positions and orientations of objects within a rough 120 cm \times 60 cm planar workspace. For both the *open* and *close* tasks, we randomize the 6D grasp pose of the gripper to evaluate each method’s robustness to variations in grasp configuration. Figure 6 provides a visual overview of the evaluated objects, and quantitative results are reported in Table II.

Looking for comparisons, the most directly comparable method would be [7] but they do not release checkpoints or inference code. Instead, we compare two variants of the π_0 model [1] with **Our** proposed approach employing a V-JEPA ViT-L backbone trained over EmbodiSwap data in Table II. The π_0 (**30**) baseline refers to the π_0 network fine-tuned over 30 in-lab collected demonstrations (we use default training settings, aside from an action horizon of 3 and 5000 training steps. The π_0 (**ES**) baseline refers to the pretrained vision backbone of π_0 network fine-tuned over the data produced by EmbodiSwap, without any access to in-lab robot demonstrations.

V. DISCUSSION AND FUTURE WORK

We compare 13 different vision backbones on the task of forecasting end effector trajectories associated with egocentric video and report results in Table I. V-JEPA (ViT-L) outperforms all vision backbones outside the class of V-JEPA models. The networks trained over large-scale robot data (RoboFlamingo, π_0 , Octo) are among the least competitive, indicating that learning over the distribution of robot trajectories is not helpful in predicting trajectories associated with egocentric video. Curiously, we notice the second most competitive network aside from V-JEPA is DINOV2 [26] - which shares a similarity with V-JEPA in that they are both pre-trained over the task of feature-level prediction.

We train π_0 on 30 in-lab demonstrations per action and compare against the performance of **Our** method (V-JEPA over ViT-L with EmbodiSwap data) in Table II. We observe that quantitatively **Our** approach produces better predictions over all actions. Furthermore, upon qualitative observation we observe that the trajectories of **Our** method appear better formed. We observe that π_0 commonly fails even for objects trained over, likely due to too few demonstrations (the authors of [1] do not state a minimum, but 30 appears insufficient). We observe that the performance of π_0 is sensitive to end-effector orientation: it succeeds when the end-effector orientation aligns with the required motion for *open/close*, and fails otherwise. Training π_0 instead over EmbodiSwap data makes π_0 (**ES**) competitive on *open*, but it still lags on *close*, *pour*, *cut*, and *place* (Table II). The main failure modes of **Our** method are: (i) joint singularities causing shutdowns; (ii) self-occlusions that remove critical visual cues; and (iii) visually plausible but unsuccessful trajectories

(e.g., narrowly missing the receptacle when *pouring*). (i) can be mitigated by predicting in robot joint space to avoid singularities and (ii) can be mitigated by using multiple perspectives as input during inference; we leave these to future work.

Results across Tables I and II support the intuition that lower hand-forecasting error correlates with real-world success: our method (V-JEPA, ViT-L) achieves 34%/15% lower translational/rotational error than π_0 within Table I and achieves a 54% higher success rate when deployed in the real world within Table II. We find this encouraging, as it implies that advancements in the task of forecasting human trajectories are directly transferrable into robot learning.

Future work involves leveraging 3D object modeling, particularly for tasks where in-hand manipulation is required. Another interesting avenue of exploration involves the composition of our trained policies within higher-level cognitive frameworks [36]. There are many possible future directions for this work, and we encourage others to use the released data, code and models.

REFERENCES

- [1] K. Black et al., “ π_0 : A vision-language-action flow model for general robot control,” *arXiv preprint arXiv:2410.24164*, 2024.
- [2] M. Lepert, J. Fang, and J. Bohg, “Phantom: Training robots without robots using only human videos,” *arXiv preprint arXiv:2503.00779*, 2025.
- [3] K. Higuchi, C. Uhde, G. Cheng, I. G. Ramirez-Alpizar, G. Venture, and N. Yamanobe, “End-to-end visuomotor learning from virtual environment to real robot,” in *2024 IEEE 20th International Conference on Automation Science and Engineering (CASE)*, IEEE, 2024, pp. 2421–2427.
- [4] R. Hoque, P. Huang, D. J. Yoon, M. Sivapurapu, and J. Zhang, “Egodox: Learning dexterous manipulation from large-scale egocentric video,” *arXiv preprint arXiv:2505.11709*, 2025.
- [5] N. Jaquier et al., “Transfer learning in robotics: An upcoming breakthrough? a review of promises and challenges,” *The International Journal of Robotics Research*, vol. 44, no. 3, pp. 465–485, 2025.
- [6] A. Bardes et al., “V-jepa: Latent video prediction for visual representation learning,” 2023.
- [7] J. Shi et al., “Zeromimic: Distilling robotic manipulation skills from web videos,” *arXiv preprint arXiv:2503.23877*, 2025.
- [8] O. M. Team et al., “Octo: An open-source generalist robot policy,” *arXiv preprint arXiv:2405.12213*, 2024.
- [9] E. Dessalene, C. Devaraj, M. Maynord, C. Fermüller, and Y. Aloimonos, “Forecasting action through contact representations from first person video,” *IEEE Transactions on Pattern Analysis and Machine Intelligence*, vol. 45, no. 6, pp. 6703–6714, 2021.

[10] S. Liu, S. Tripathi, S. Majumdar, and X. Wang, “Joint hand motion and interaction hotspots prediction from egocentric videos,” in *Proceedings of the IEEE/CVF Conference on Computer Vision and Pattern Recognition*, 2022, pp. 3282–3292.

[11] J. Ma, W. Bao, J. Xu, G. Sun, X. Chen, and H. Wang, “Novel diffusion models for multimodal 3d hand trajectory prediction,” *arXiv preprint arXiv:2504.07375*, 2025.

[12] H. G. Singh et al., “Hand-object interaction pretraining from videos,” in *2025 IEEE International Conference on Robotics and Automation (ICRA)*, IEEE, 2025, pp. 3352–3360.

[13] F. Lin, Y. Hu, P. Sheng, C. Wen, J. You, and Y. Gao, “Data scaling laws in imitation learning for robotic manipulation,” *arXiv preprint arXiv:2410.18647*, 2024.

[14] J. Yang, B. Liu, J. Fu, B. Pan, G. Wu, and L. Wang, “Spatiotemporal predictive pre-training for robotic motor control,” *arXiv preprint arXiv:2403.05304*, 2024.

[15] V. Liu et al., “Egozero: Robot learning from smart glasses,” *arXiv preprint arXiv:2505.20290*, 2025.

[16] M. Lepert, J. Fang, and J. Bohg, “Masquerade: Learning from in-the-wild human videos using data-editing,” *arXiv preprint arXiv:2508.09976*, 2025.

[17] H. Alwassel, F. C. Heilbron, V. Escorcia, and B. Ghanem, “Diagnosing error in temporal action detectors,” in *Proceedings of the European conference on computer vision (ECCV)*, 2018, pp. 256–272.

[18] J. Zhang, J. Deng, C. Ma, and R. A. Potamias, “Hawor: World-space hand motion reconstruction from egocentric videos,” in *Proceedings of the Computer Vision and Pattern Recognition Conference*, 2025, pp. 1805–1815.

[19] L. Piccinelli et al., “Unidepthv2: Universal monocular metric depth estimation made simpler,” *arXiv preprint arXiv:2502.20110*, 2025.

[20] N. Ravi et al., “Sam 2: Segment anything in images and videos,” *arXiv preprint arXiv:2408.00714*, 2024.

[21] A. Darkhalil et al., “Epic-kitchens visor benchmark: Video segmentations and object relations,” *Advances in Neural Information Processing Systems*, vol. 35, pp. 13 745–13 758, 2022.

[22] R. Wei et al., “Omnieraser: Remove objects and their effects in images with paired video-frame data,” *arXiv preprint arXiv:2501.07397*, 2025.

[23] J. Romero, D. Tzionas, and M. J. Black, “Embodied hands: Modeling and capturing hands and bodies together,” *arXiv preprint arXiv:2201.02610*, 2022.

[24] E. Dessalene, M. Maynard, C. Fermüller, and Y. Aloimonos, “Therbligs in action: Video understanding through motion primitives,” in *Proceedings of the IEEE/CVF Conference on Computer Vision and Pattern Recognition*, 2023, pp. 10 618–10 626.

[25] K. He, X. Chen, S. Xie, Y. Li, P. Dollár, and R. Girshick, “Masked autoencoders are scalable vision learners,” in *Proceedings of the IEEE/CVF conference on computer vision and pattern recognition*, 2022, pp. 16 000–16 009.

[26] M. Oquab et al., “Dinov2: Learning robust visual features without supervision,” *arXiv preprint arXiv:2304.07193*, 2023.

[27] S. Nair, A. Rajeswaran, V. Kumar, C. Finn, and A. Gupta, “R3m: A universal visual representation for robot manipulation,” *arXiv preprint arXiv:2203.12601*, 2022.

[28] Y. J. Ma, S. Sodhani, D. Jayaraman, O. Bastani, V. Kumar, and A. Zhang, “Vip: Towards universal visual reward and representation via value-implicit pre-training,” *arXiv preprint arXiv:2210.00030*, 2022.

[29] A. Majumdar et al., “Where are we in the search for an artificial visual cortex for embodied intelligence?” *Advances in Neural Information Processing Systems*, vol. 36, pp. 655–677, 2023.

[30] X. Li et al., “Vision-language foundation models as effective robot imitators,” *arXiv preprint arXiv:2311.01378*, 2023.

[31] C. Ryali et al., “Hiera: A hierarchical vision transformer without the bells-and-whistles,” in *International conference on machine learning*, PMLR, 2023, pp. 29 441–29 454.

[32] D. Damen et al., “Rescaling egocentric vision: Collection, pipeline and challenges for epic-kitchens-100,” *International Journal of Computer Vision*, vol. 130, no. 1, pp. 33–55, 2022.

[33] Y. Liu et al., “Hoi4d: A 4d egocentric dataset for category-level human-object interaction,” in *Proceedings of the IEEE/CVF Conference on Computer Vision and Pattern Recognition*, 2022, pp. 21 013–21 022.

[34] K. Grauman et al., “Ego4d: Around the world in 3,000 hours of egocentric video,” in *Proceedings of the IEEE/CVF conference on computer vision and pattern recognition*, 2022, pp. 18 995–19 012.

[35] A. P. Lindvig, I. Iturrate, U. Kindler, and C. Sloth, “Urrtde: An interface for controlling universal robots (ur) using the real-time data exchange(rtde),” in *2025 IEEE/SICE International Symposium on System Integration (SII)*, 2025, pp. 1118–1123. DOI: 10.1109/SII59315.2025.10871000

[36] M. Beetz, G. Kazhoyan, and D. Vernon, “Robot manipulation in everyday activities with the cram 2.0 cognitive architecture and generalized action plans,” *Cognitive Systems Research*, p. 101 375, 2025.